PCCP



View Article Online **PAPER**



Cite this: Phys. Chem. Chem. Phys., 2025, 27, 2033

Optimization of nonlinear properties of C₆O₆Li₆-doped alkalides via group I/III doping for unprecedented charge transfer and advancements in optoelectronics†

Naveen Kosar, *a Khurshid Ayub, (10 b Abdulaziz A. Al-Saadi, (10 cd

The design and synthesis of nonlinear optical (NLO) materials are rapidly growing fields in optoelectronics. Considering the high demand for newly designed materials with superior optoelectronic characteristics, we investigated the doping process of Group-IIIA elements (namely, B, Al and Ga) onto alkali metal (AM = Li, Na and K)-supported $C_6O_6Li_6$ (AM@ $C_6O_6Li_6$) complexes to enhance their NLO response. The AM-C₆O₆Li₆ complexes retained their structural features following interaction with the Group-IIIA elements. Interaction energies as high as -109 kcal mol⁻¹ demonstrated the high thermodynamic stability of these complexes. An exceptional charge transfer behavior was predicted in these complexes, where the electronic density of the Group-III metals shifted toward the alkali metals, making these complexes behave as alkalides. The π conjugation of $C_6O_6Li_6$ was found to withdraw excess electrons from the Group IIIA metals in these alkalides, which were subsequently transferred to the Group IA metals. The energy gap of the frontier molecular orbitals (FMOs) in the AM-C₆O₆Li₆ complexes was notably reduced upon alkalide formation. UV-visible analysis explicitly showed a bathochromic shift in the alkalides. The first hyperpolarizability (β_0) was calculated to confirm the NLO properties of these alkalides. $B-C_6O_6Li_6-K$ exhibited the highest β_0 value of 1.75 imes 10⁵ au. The vibrational frequencydependent first and second hyperpolarizability values illustrated an increase in hyperpolarizability at a frequency of 532 nm. A higher n_2 value of 8.39×10^{-12} cm 2 W $^{-1}$ was obtained for B-C $_6$ O $_6$ Li $_6$ -Na at 532 nm. These results highlight the promising NLO response of the designed alkalides and their potential applications in the field of optics.

Received 10th October 2024, Accepted 22nd December 2024

DOI: 10.1039/d4cp03890h

rsc.li/pccp

1. Introduction

Generation of excess electrons in a complex is a promising technique for enhancing the nonlinear optical (NLO) response of materials. 1-8 NLO materials are on high demand due to their extensive applications in fields such as optics,7-9 electronics, 10,11 bioimaging 12,13 and memory storage devices. 14,15 Various techniques are adopted to generate diffuse excess electrons, with the most widely known being the doping of electropositive metals onto a suitable substrate. 16,17 The substrate holds the incoming diffuse excess electrons from the metals. After the diffusion of electrons, the geometric, electronic and optical properties are effectively tuned. To date, Group-IA^{18–21} metals, Group-IIA metals,²² transition metals²³ and superalkalis^{24,25} have been used as sources for the generation of excess electrons. The metal-supported surfaces are further classified as electrides^{26,27} earthides,²⁸ metalides^{29,30} and alkalides.³¹ In electrides, the excess electrons occupy the free space between the interacting metals and the surface, while in alkalides, the electrons shift to the alkali metals. Literature suggests that alkalides exhibit superior NLO responses. Extensive research has been performed on alkalides as effective NLO materials. For example, Sun et al. designed transition and alkali metal-doped adz alkalides, which exhibited a higher β_0 value of

^a Department of Chemistry, University of Management and Technology (UMT), C-11, Iohar Town Lahore, Pakistan, E-mail: naveen.kosar@umt.edu.nk

^b Department of Chemistry, COMSATS University Islamabad, Abbottabad Campus, Abbottabad-22060, Pakistan, E-mail: mahmood@cuiatd.edu.pk

^c Chemistry Department, King Fahd University of Petroleum & Minerals, Dhahran 31261, Saudi Arabia

^d Interdisciplinary Research Center for Refining and Advanced Chemicals, King Fahd University of Petroleum & Minerals, Dhahran 31261, Saudi Arabia

^e Research Center for Advanced Materials Science (RCAMS), Chemistry Department, Faculty of Science, King Khalid University, P.O. Box 9004, Abha 61413, Saudi

f Department of Chemistry, College of Science, University of Bahrain, P.O. Box 32038, Sakhir, Bahrain

[†] Electronic supplementary information (ESI) available. See DOI: https://doi.org/ 10.1039/d4cp03890h

 6.16×10^4 au. They further applied the same metal doping to TriPip222, where β_0 effectively increased to 1.80 \times 10⁵ au. Li and coworkers reported alkaline earth metal-doped amine alkalides with β_0 values up to 1.23×10^5 au. ³² Li *et al.* designed alkali metal-doped graphene, graphdiyne and graphyne-based alkalides, with the alkali metal-doped graphdiyne exhibiting the highest β_0 value of 3.93 \times 10⁵ au among these complexes.³³

Recent literature reports on enhancement of NLO responses through the doping of metals on various surfaces is leading toward the development of new alkalides with better NLO properties. Chen et al. designed alkali metaldoped calix[4]pyrrole alkalides. A Li⁺@(calix[4]pyrrole)K⁻ alkalide has a higher hyperpolarizability than that of the Li⁺@(calix[4]pyrrole)e⁻ electride.³⁴ Li and co-workers modelled alkali/superalkali-based calix[4]pyrrole alkalides. The β_0 value of these alkalides was increased up to 3.47×10^3 au compared to pure calix[4]pyrrole.35 Li and colleagues suggested that an alkali metal-doped N₃H₃ complex may have enhanced NLO response because the hyperpolarizability of this complex is 6.27×10^4 au.³⁶ Banerjee and Nandi designed alkalides based on alkali metal-doped calcium chain structures with extraordinary NLO properties with β_0 ranging from 1.57 \times 10⁴ to 1.61×10^6 au.³⁷ Ayub and co-workers explored judicious placement of alkali and alkaline earth metals on the hydrogen and fluorine faces of the F₆C₆H₆ surface, respectively. A maximum β_0 value of 2.91 \times 10⁴ au was notified in these complexes.²⁸ Kang et al. observed the alkalide properties of alkali metaldoped open cage C₅₀N₅H₅ fullerenes having good NLO response (β_0 values up to 1.91 \times 10⁵ au).³⁸ Wang et al. theoretically studied the NLO response of alkali and alkaline earth metal-doped Janus-type structures under an applied electric field and observed a high hyperpolarizability value in the range of 5.9×10^4 to 6.4×10^4 au. ³⁹ Sohaib et al. investigated the NLO properties of alkali metals doped with stacked Janus-type alkalides and reported a very large first hyperpolarizability of 5.13×10^7 au. 40 Mahmod and colleagues worked on the alkali and alkaline earth metal-doped C₆O₆Li₆ complexes where Mg- $C_6O_6Li_6$ -K has the highest β_0 value of 1.75 \times 10⁵ au.⁴¹

Group-1A and group-IIA elements are effectively used as metal sources to acquire a high NLO response. Because these elements have low ionization potential and can easily donate excess electrons, which can enhance the NLO response of a system. However, the doping of Group-IIIA metals with Group-IA metals is not considered so far. Based on their individual doping influence on tuning the NLO response of different surfaces, we deemed to search their doping nature with both Group-I/III metals. We infer the withdrawal of diffuse excess electrons from Group IIA metals to alkali metals via the C₆O₆Li₆ surface, which may give rise to the alkalide properties manifested in these investigated complexes. The alkalide properties of the Group-IA and Group-IIIA element-doped C₆O₆Li₆ surface were evaluated. We hope that these investigated alkalides can be used as extraordinary NLO nanomaterials for the nextgeneration optics. C₆O₆Li₆ is suggested to be a good supportive surface for alkali metals, 42 alkaline earth metals, 43 alkali and alkaline earth metals, 41 transition metals, 44 and super alkalis, 45 which is used for optics, 46 electronics, 47 storage of hydrogen, 48,49 etc. Group-IIIA metals can also eject their electrons to generate diffuse excess electrons, and this system can be used as effective NLO materials. According to the literature, the ejection of electrons from boron atoms requires high-energy laser light, elevated temperatures, and UV photons. 50-53 However, we propose that the current strategy of modeling novel alkalides through the doping of Group-IA and Group-IIIA metals on C6O6Li6 may offer a more energetically favorable approach. In this context, Group-IIIA metals can readily eject their electrons, which then accumulate on the alkali metals, thereby inducing alkalide properties in these complexes. The structural, electronic, and nonlinear optical (NLO) properties of these alkalides were investigated using density functional theory (DFT). Furthermore, we suggest that the NLO response of C₆O₆Li₆ can be further enhanced through this doping strategy.

2. Computational methodology

The optimization and frequency analyses of individual C₆O₆Li₆ and Group-IA & Group-IIIA metal-doped C6O6Li6 were carried out by the ω B97XD/6-31+G(d,p) method of DFT. All the simulations were executed using the Gaussian 09 package, 54 whereas the results are analyzed using the GaussView 5.0 package. 55 These analyses confirmed the energy minimization of all geometries with no imaginary frequency. Zero-point corrected vibrational energies were obtained from the analyses to calculate the interaction energy of all the complexes. The interaction energy of Group-IA & Group-IIIA metals with C6O6Li6 was obtained using eqn (1):

$$E_{\text{int}} = E_{\text{G-IA/G-IIIAC}_6O_6\text{Li}_6} - (E_{\text{C}_6O_6\text{Li}_6} + E_{\text{G-IA/G-IIIA}})$$
 (1)

Natural bond orbital (NBO) and electronic density difference (EDD) analyses were performed to estimate the charge transfer between the metals and C₆O₆Li₆ in each alkalide. To understand the electronic properties, the energy difference between frontier molecular orbitals (E_{H-L}) was calculated using eqn (2):

$$E_{\rm H-L} = E_{\rm L} - E_{\rm H} \tag{2}$$

The static second hyperpolarizability (γ_0) , the first hyperpolarizability (β_0) and polarizability (α_0) were calculated at ω B97XD/ 6-31+G(d,p) to estimate the NLO response. This ωB97XD density functional and 6-31+G(d,p) Pople basis set are important for the estimation of optical and nonlinear optical properties of complexes. 56-59 Literature reveals the importance of density functionals in accurately describing the NLO properties of the metal-doped complexes based on the %HF exchange parameter in these functionals. Nowadays, computational chemists primarily apply ωB97XD to estimate the nonlinear optical properties of NLO nanomaterials. ωB97XD is a long-range corrected hybrid density functional with a dispersion correction density functional, which contains 100% HF exchange and performs exceptionally well for assessing NLO properties through the calculations of first hyperpolarizability. Among the Pople basis sets, especially medium-sized basis sets' 6-31+G(d,p) gave

better results and was suggested to be a suitable basis set for the estimation of the first hyperpolarizability.⁶⁰ The α_0 , β_0 and γ_0 values of all complexes were obtained using the following equations:

$$\alpha_0 = \frac{1}{3} (\alpha_{xx} + \alpha_{yy} + \alpha_{zz}) \tag{3}$$

$$\beta_0 = \left[\beta_x^2 + \beta_y^2 + \beta_z^2\right]^{\frac{1}{2}} \tag{4}$$

Here,

$$\beta_x = \beta_{xxx} + \beta_{xyy} + \beta_{xzz}, \quad \beta_y = \beta_{yyy} + \beta_{yzz} + \beta_{yxx}, \quad \beta_z = \beta_{zzz} + \beta_{zxx} + \beta_{zyy},$$

$$Y_0 = \frac{1}{5} \left[Y_{xxxx} + Y_{yyyy} + Y_{zzzz} + 2 \left(Y_{xxyy} + Y_{xxzz} + Y_{yyzz} \right) \right]$$
 (5)

Frequency (ω) -dependent NLO properties of the complexes were also determined, which are important for experimentalists when they work on complexes in the lab work. For this purpose, the calculations were carried out at routinely used laser wavelengths of 532 nm and 1064 nm.61,62 Frequency-dependent hyperpolarizability contains the approximation of electrooptic Pockel's effect (EOPE) $\beta(-\omega; \omega, 0)$ and second harmonic generation $\beta(-2\omega; \omega, \omega)$. Electric field-induced second harmonic generation $(\gamma(-2\omega; \omega, \omega, 0))$, dc-Kerr effect $\gamma(-\omega; \omega, 0, 0)$ and degenerate four-wave mixing ($\gamma DFWM(\omega)$) were calculated for the estimation of frequency-dependent second hyperpolarizability $(\gamma(\omega))$. The mathematical equations for $\beta(\omega)$, SHG (β_i) , and EOPE (β_i) were given using the following equations:

$$\beta(\omega) = \left[\beta_{x^2} + \beta_{y^2} + \beta_{z^2}\right]^{1/2} \tag{6}$$

$$\beta_{i}(SHG) = \beta_{iii}(-2\omega, \omega, \omega) + \beta_{ijj}(-2\omega, \omega, \omega) + \beta_{ikk}(-2\omega, \omega, \omega)$$
(7)

$$\beta_{i}(\text{EOPE}) = \beta_{iii}(-\omega, \omega, 0) + \beta_{ijj}(-\omega, \omega, 0) + \beta_{ikk}(-\omega, \omega, 0)$$
(8)

The second hyperpolarizability coefficients including static $(\gamma(0; 0, 0, 0))$, ESHG $(\gamma(-2\omega; \omega, \omega, 0))$ and dc-Kerr $(\gamma(-\omega; \omega, \omega, 0))$ $(\omega, 0)$) were also calculated. The degenerate four-wave mixing $(\gamma^{\text{DFWM}}(\omega))$ equation was suggested by Tarazkar *et al.* in 2014,⁶³ as given below.

$$\begin{split} \gamma^{\mathrm{DFWM}}(-\omega;\omega,-\omega,\omega) &\approx \left(\frac{1}{3}\right) \gamma(-2\omega;\omega,\omega,0) \\ &+ \left(\frac{1}{3}\right) \gamma(-\omega;\omega,0,0) \\ &+ \left(\frac{1}{3}\right) \gamma(0;0,0,0) \end{split} \tag{9}$$

Additionally, the quadratic nonlinear refractive index $(n_2)^{64}$ of all complexes was obtained using eqn (10):

$$n^2 (\text{cm}^2 \text{ W}^{-1}) = 8.28 \times 10^{-23} \gamma^{\text{DFWM}}$$
 (10)

We undergo a benchmark study of interaction energies and NLO properties using different methods to further ensure the accuracy of our method for the designed complexes. For this study, we also simulated all the complexes on LC-BLYP⁶⁵ which is the long-range corrected density functional of the DFT. The

simulations with LC-BLYP and ωB97XD are implemented with Dunning's aug-cc-PVDZ⁶⁶ and aug-cc-PVTZ⁶⁷ basis sets and Karlsruhe's def2-TZVP basis set. 68,69 The results obtained at ωB97XD with 6-31+G(d,p) are more reliable, and these results are given in the main manuscript, while the results of the other basis sets are given in ESI† (ESI.† Tables S1 and S2). The augccPVDZ and aug-cc-PVTZ basis sets show error when implemented on K containing complexes, as the atomic size of the K is out of reach of these dunning basis sets (aug-ccPVDZ and aug-cc-PVTZ basis sets). The total density of state spectra were generated through the GaussSam software to validate the energy states of molecular orbitals. Two-level model analysis was implemented to rationalize the internal factors responsible for the enhancement in NLO response. Furthermore, crucial excited states are analyzed using the TD-DFT method at the same level of theory.

Results and discussions

The pristine C₆O₆Li₆ structure was evaluated first where sixmembered rings of C, Li and O are linked together to form C₆O₆Li₆ with a planar star-shaped structure. The point group symmetry of $C_6O_6Li_6$ is D_{6h} . The C-O, O-Li, and C-C bond lengths in C₆O₆Li₆ are 1.38 Å, 1.79 Å, and 1.41 Å, respectively. Our calculated bond lengths are comparable to the one already reported in the literature.42

3.1. Structural and thermal stability of group-I and III metaldoped C₆O₆Li₆ alkalides

Nine complexes are designed by doping Group-I (K, Na, Li) and Group-III (Ga, Al, B) metals on the C₆O₆Li₆ surface, and the structures of pristine and doped complexes are given in Fig. 1. Selected metals from Group-IA and Group-IIIA prefer to reside on the top of the central hexagonal ring of C6O6Li6 except Li and Na metal-doped Group-IIIA@C6O6Li6 alkalides. Li and Na metals have smaller atomic sizes than potassium and prefer to be adsorbed onto one side of C₆O₆Li₆. The behavior is similar to alkali and alkaline earth metal-doped C₆O₆Li₆ complexes. ⁴¹ The interaction distances of Group-IIIA metals from the central position of C₆O₆Li₆ are 1.60, 1.45, 1.46, 1.99, 2.04, 2.00, 2.11, 2.05, and 2.06 Å in B-C₆O₆Li₆-K, B-C₆O₆Li₆-Na, B-C₆O₆Li₆-Li, Al-C₆O₆Li₆-K, Al-C₆O₆Li₆-Na, Al-C₆O₆Li₆-Li, Ga-C₆O₆Li₆-K, Ga-C₆O₆Li₆-Na, and Ga-C₆O₆Li₆-Li, respectively. Moving towards the adsorption sites of the alkali metals, it is noticed that the K metal holds the central position on C₆O₆Li₆ (opposite Group-IIIA metals). The interaction distances of potassium from the central position of C₆O₆Li₆ are 3.33, 3.24, and 3.15 Å in B-C₆O₆Li₆-K, Al-C₆O₆Li₆-K, and Ga-C₆O₆Li₆-K, respectively. The average interaction distances of Li and Na metals from Li metals of the adsorption sides are 3.33, 3.45, 3.40, 3.50, 3.34 and 3.47 Å in B-C₆O₆Li₆-Na, B-C₆O₆Li₆-Li, Al-C₆O₆Li₆-Na, Al-C₆O₆Li₆-Li, Ga-C₆O₆Li₆-Na, and Ga-C₆O₆Li₆-Li, respectively. The interatomic distance of Group-IIIA metals is increased with the increase in atomic size. The outcomes are comparable to the research report on NLO response of alkali/alkaline earth

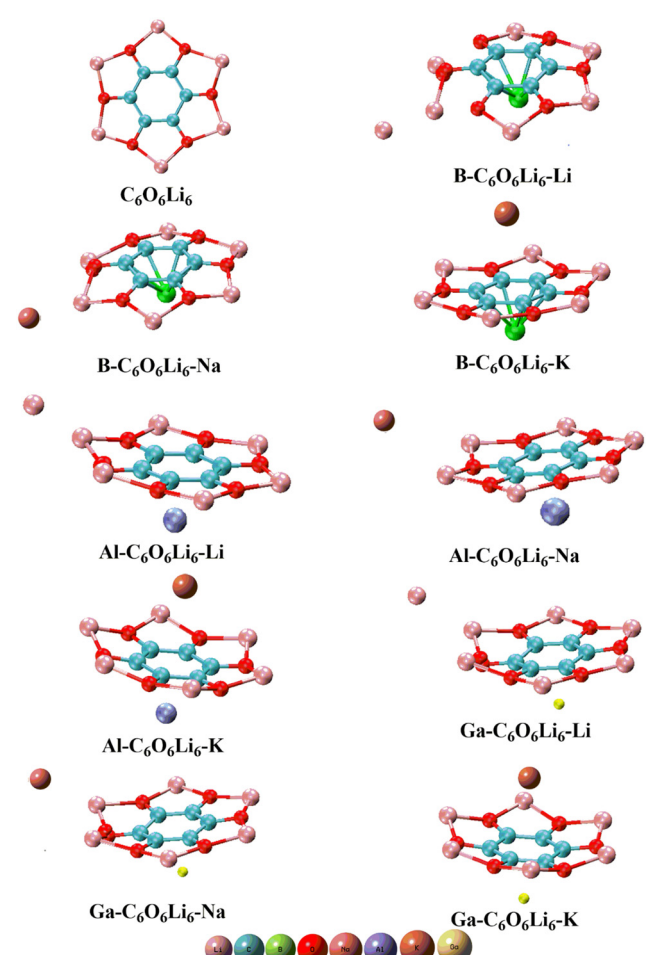


Fig. 1 Pristine C₆O₆Li₆ and group-IA and group-IIIA metal-doped C₆O₆Li₆ complexes.

metal-doped C₆O₆Li₆ complexes, where the distance between both dopants and C₆O₆Li₆ increases with the increase in the atomic size of alkali metals (from Li to K).41 However, the interatomic bond distance of alkali metals in respective complexes is decreased with the increase in atomic size. In the case of Group-IIIA metals (Ga, Al, and B), the lowest distance (1.45 Å) was calculated for B from the center of C₆O₆Li₆ in B-C₆O₆Li₆-Li. The highest interatomic distance (2.11 Å) was obtained for Ga from the center of C₆O₆Li₆ in Ga-C₆O₆Li₆-K. In the case of alkali metals (K, Na, and Li), the highest interatomic distance (6.23 Å) was obtained for Na from the center of C₆O₆Li₆ in Al-C₆O₆Li₆-Na, and the lowest interatomic distance (3.15 Å) was obtained for K from the center of C₆O₆Li₆ in Ga-C₆O₆Li₆-K

The C₆O₆Li₆ structure retains its integrity during the doping of all elements, except for the small variations observed in B-C₆O₆Li₆-Li and B-C₆O₆Li₆-Na alkalides. The reason is the displacement of the Li atom of the C₆O₆Li₆ surface towards the doped alkali metals. Li and co-workers observed a similar trend using their study on the interaction of Group-IIA metals with hexaammine.⁷⁰ The point group symmetry of C₆O₆Li₆ is changed to C1 symmetry after doping of Group-IA and IIIA metals.

Table 1 NBO charges on Group-IA metals (Q_{G-IA} in |e|), NBO charges on group-IIIA metals (Q_{G-IIIA} in |e|), interatomic distance of group-IIIA from the center of $C_6O_6Li_6$ ($d_{ring-G-IIIA}$ in Å, G-IIIA = Ga, Al, and B), interatomic distance of group-IA from the center of $C_6O_6Li_6$ ($d_{ring-G-IA}$ in Å, G-IA = K, Na, and Li), vertical ionization energy (VIE in eV) and interaction energies $(E_{\text{int}} \text{ in kcal mol}^{-1})$ of pristine $C_6O_6Li_6$ and group-I and group-III metaldoped $C_6O_6Li_6$ -alkalides (group-IA = K, Na, and Li and group-IIIA = Ga, Al, and B)

Pristine and group-I and group-III doping	$Q_{ ext{G-IA}}$	$Q_{ ext{G-IIIA}}$	$d_{ m ring ext{-}G ext{-}IIIA}$	$d_{ m ring ext{-}G ext{-}IA}$	VIE	$E_{ m int}$
$C_6O_6Li_6$	_	_	_	_	3.04	_
$B-C_6O_6Li_6-Li$	-0.29	0.11	1.46	3.33	3.75	-105.35
B-C ₆ O ₆ Li ₆ -Na	-0.31	0.12	1.45	3.45	3.62	-104.66
$B-C_6O_6Li_6-K$	-0.51	0.17	1.60	3.33	3.02	-88.13
Al-C ₆ O ₆ Li ₆ -Li	-0.38	0.65	2.00	3.40	3.72	-97.41
Al-C ₆ O ₆ Li ₆ -Na	-0.39	0.67	1.99	3.50	3.47	-97.12
Al-C ₆ O ₆ Li ₆ -K	-0.47	0.69	2.04	3.24	3.14	-89.04
Ga–C ₆ O ₆ Li ₆ –Li	-0.35	0.63	2.06	3.34	3.73	-109.13
Ga–C ₆ O ₆ Li ₆ –Na	-0.37	0.63	2.05	3.47	3.57	-108.57
Ga-C ₆ O ₆ Li ₆ -K	-0.46	0.68	2.11	3.15	3.12	-102.32

This change in symmetry was also observed by Kanis et al., and it plays an important role in the improvement of NLO response of a surface.⁷¹ This change in symmetry is common in almost all theoretical studies on NLO, specifically Wajid et al. observed such change during doping of Group-IIA43 and Group-IA42 metals on C₆O₆Li₆.

The thermodynamic stability of a complex is inferred from the interaction energy (E_{int}) . If a complex has high negative interaction energy, the complexation reaction is exothermic in nature and reflects the high thermodynamic stability of complexes. These properties confirmed the possibility of practical synthesis of these complexes. 72 To estimate the thermal stability of a complex, we also calculated the interaction energy of all complexes (see Table 1).

Ga-C₆O₆Li₆-Li, Ga-C₆O₆Li₆-Na, Ga-C₆O₆Li₆-K, Al-C₆O₆Li₆- $\text{Li, Al-C}_6\text{O}_6\text{Li}_6 - \text{Na, Al-C}_6\text{O}_6\text{Li}_6 - \text{K, B-C}_6\text{O}_6\text{Li}_6 - \text{Li, B-C}_6\text{O}_6\text{Li}_6 - \text{Na,} \\$ and B-C₆O₆Li₆-K complexes have E_{int} of, -109.13, -108.57, -102.32, -97.41, -97.12, -89.04, -105.35, -104.66, and $-88.13 \text{ kcal mol}^{-1}$, respectively at $\omega B97XD$ by the 6-31+G(d,p) method. The negative E_{int} value of our designed complexes reflects the thermal stability and energetic favorability of complexation reactions. Pristine and doped complexes are also optimized by the LC-BLYP/aug-cc-PVDZ, ωB97XD/aug-cc-PVDZ, LC-BLYP/aug-cc-PVTZ, ωB97XD/aug-cc-PVTZ, LC-BLYP/ def2-TZVP, and ω B97XD/def2-TZVP methods. A higher E_{int} value was obtained at the ωB97XD/6-31+G(d,p) level, which is given in main manuscript. The E_{int} values obtained by the other methods are given in the ESI† (ESI.† Table S1). The aug-ccPVDZ and aug-cc-PVTZ basis sets show error when implemented on K-containing complexes as the atomic size of K is out of reach of these dunning basis sets (aug-ccPVDZ and aug-cc-PVTZ basis sets).

Considering the interaction energies of both Group-IA metals, we observed a monotonic trend of decreasing interaction energy with the increase in the atomic number of Group-IA metals. The interaction energy decreases with the increase in the atomic size of the alkali metals, and subsequently their

stability decreases. Among all metals, Li has the shorter interatomic distance from the adsorption side of the C₆O₆Li₆ ring in each of Li-C₆O₆Li₆@ Group-IIIA complexes, which is the reason for the strong interactions between Li and C6O6Li6@ Group-IIIA, and ultimately for the thermal stabilities of these Li-doped complexes. The trend of lowering interaction energy with the increase in atomic size is also observed during alkali and alkaline earth metal doping of the same C₆O₆Li₆ surface.⁴¹ A nonmonotonic trend is seen among the Group-IIIA metals, and the interaction energy decreases from B to Al but increases in the case of Ga. The reason for the nonmonotonic behavior of the Group-IIIA metals is the smaller atomic size of B, which formed bond with C₆O₆Li₆ that is validated from its shorter distance. Ga has a larger atomic size, and it can easily donate the electronic density and form stronger interactions with C₆O₆Li₆, and these Ga-C₆O₆Li₆-Alkali-IA alkalides have more interaction energy than others.

Overall, the Ga-C₆O₆Li₆-Li complex is the most stable based on its highest interaction energy $(-109.13 \text{ kcal mol}^{-1})$. The atomic size of gallium is large, and it can easily donate electronic density to the C₆O₆Li₆ surface. The surface becomes polarized and electron rich, and the interaction between two highly charged species is strong. This leads to a higher interaction energy in the case of Ga. However, smaller lithium metals interact on one side of the polarized C6O6Li6 surface to complete its outer shell. These stronger interactions are the reasons for the more chemical stability of the Ga-C6O6Li6-Li complex. Similar results are reported in the previous study of Group-IA⁷³ and Group-IIA metal⁷⁴-doped complexes. In alkali metal-doped gallium nitride nanocages, the stronger interaction is seen for lithium-doped complexes by Khurshid et al. 15

3.2 NBO and EDD analyses of group-I/IIIA metal-doped C₆O₆Li₆ alkalides

NBO analysis is used to understand the shifting of charge from the metal toward surface or vice versa. In all complexes, Group-IIIA metals have a positive charge that ranges from 0.11 to 0.69|e|. The highest charge (0.69|e|) for Al was obtained in Al- $C_6O_6Li_6$ -K and the lowest (0.11|e|) was obtained for Li in B-C₆O₆Li₆-Li. Interestingly, the Group-IA metals have negative charges between -0.29 and -0.51|e|. The positive NBO values on Group-IIIA metals reflect that π conjugation of C₆O₆Li₆ withdraws excess electrons from Group-IIIA metals in these alkalides. These excess electrons are then transferred to Group-IA metals and these metals have negative NBO values. This shift of excess electrons from Group-IIIA metals to Group-IA metals is based on electron push-pull mechanism. In the literature, it is mentioned that high energy laser light, high heat and UVphotons are required to eject electrons from the Boron atom, ⁷⁶ but our current strategy of metal doping with supportive C₆O₆Li₆ makes it possible with high energetic and electronic feasibility. Both types of Group-IA metals get stable noble gas electronic configuration through this push-pull mechanism and form electronically stable alkalides. The negative charges on Group-IA metals justify their alkalide properties.

Table 2 First hyperpolarizability (β_0 in au), polarizability (α_0 in au), dipole moment (μ in Debye), HOMO-LUMO energy gap ($E_{\rm L-H}$ in eV), energies of LUMO (E_{LUMO}), and HOMO (E_{HOMO}) of the pristine $C_6O_6Li_6$ and group-I and group-III metal-doped $C_6O_6Li_6$ -alkalides (group-I = K, Na, and Li; group-III = Ga, Al, and B)

-4.39 -3.75
2 75
-3./3
-3.62
-3.02
-3.72
-3.47
-3.14
-3.73
-3.57
-3.12

As we discussed above, doping of Group-I/IIIA metals causes variation in the dipole moment of C₆O₆Li₆ which is zero in pristine form. When metals are doped on C₆O₆Li₆, the shifting of charges occurs as a result of huge charge separation. This separation increases the dipole moment of the investigated alkalides, which also increases except B-C₆O₆Li₆-K alkalides. Beside charge separation, the interatomic distance between Group-I/IIIA and surface (C₆O₆Li₆) results in an increase in the dipole moment of alkalides compared to pristine C₆O₆Li₆. The μ_0 values of B-C₆O₆Li₆-K, B-C₆O₆Li₆-Na, B-C₆O₆Li₆-Li, Al-C₆O₆Li₆-K, Al-C₆O₆Li₆-Na, Al-C₆O₆Li₆-Li, Ga-C₆O₆Li₆-K, Ga- $C_6O_6Li_6$ -Na and $Ga-C_6O_6Li_6$ -Li alkalides are 5.98, 16.46, 15.80, 5.00, 18.31, 16.83, 5.73, 16.61, and 15.58 D, respectively (Table 2). Al-C₆O₆Li₆-Na has the highest μ_0 value of 18.31 D among all alkalides because the charge separation in this alkalide is larger than that of other alkalides.

EDD analysis was also performed to understand the charge transfer in designed alkalides through qualitative pictorial representation (see Fig. 2). The two types of iso surfaces were generated on each of the complexes. Both are differentiated on the basis of purple color and blue color iso surfaces where purple represents the rich electron density region and cyan blue represents the poor electronic density region. The generation of iso surfaces between the interacting species in each of the complex represents the shifting of charge density after complexation. The cyan blue color iso surface is toward the Group-IA metals in each of the complexes, whereas the purple color iso surface has appeared towards C₆O₆Li₆ that confirmed the charge transfer from G-IIIA-C₆O₆Li₆ to the Group-IA metals.

3.3. FMO analysis and alkalide properties of group-I/III metaldoped C₆O₆Li₆

FMO analysis was performed to understand the electronic stability and conductivity of pristine C₆O₆Li₆ and Group-I/IIIA metal-doped complexes (see Table 2). Pristine C₆O₆Li₆ has an energy gap (E_{H-L}) of 4.63 eV. When Group-I/IIIA metals are doped on pristine $C_6O_6Li_6$, the E_{H-L} value is reduced to be in the range of 2.72 eV to 3.54 eV. The lowest gap of 2.72 eV is seen for B-C₆O₆Li₆-K. For the B-C₆O₆Li₆-K complex, the E_{HOMO} , E_{LUMO} and $E_{\text{H-L}}$ values are -3.02, -0.29, and 2.72 eV,

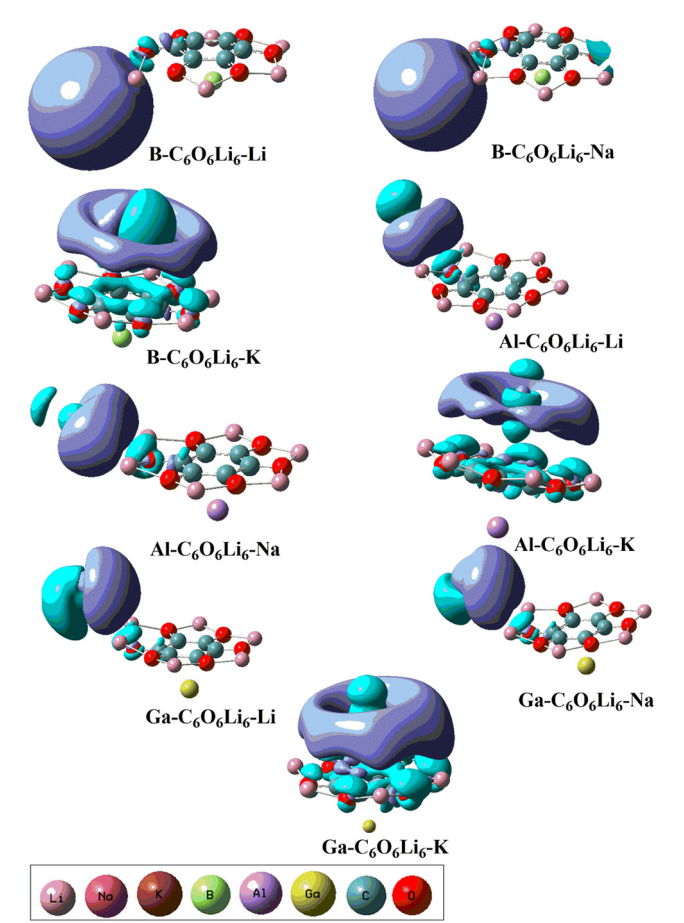


Fig. 2 EDD analysis for group-IA and group-IIIA metal-doped C₆O₆Li₆ alkalides representing electron-rich and electron-poor iso surface regions at an isovalue of 0.04 au

respectively. The decreased H-L gap is attributed to the increase in the energy of new occupied orbitals and the decrease in the energy of new unoccupied orbitals. The decrease in the energy gap confirmed the semiconductive properties of these alkalides with sufficient thermal stability. Li and coworkers in their work on the NLO response of N₃H₃ with alkali metals reported a similar type of behavior.⁷⁷

The isodensities of the highest occupied and the lowest unoccupied frontier orbitals are also studied, and their graphics are given in Fig. 3. It is observed that HOMO isodensities are present on Group-IA metals and LUMO isodensities are located on the Group-IIIA metals. The anionic alkali metals with HOMO densities reflect the alkalide behavior of the investigated complexes. The presence of HOMOs densities on metals justifies alkalide characteristics. Here, the electron push-pull mechanism is operated in each complex where the π conjugation of C₆O₆Li₆ withdraws valence shell electrons from the Group-IIIA metals and these electrons act as excess electrons. Meanwhile, these excess electrons are shifted to the alkali metals doped on the other side of C₆O₆Li₆. The outcomes are more comparable to the research work on alkalide properties of diamantanes with alkali metals.⁷⁸

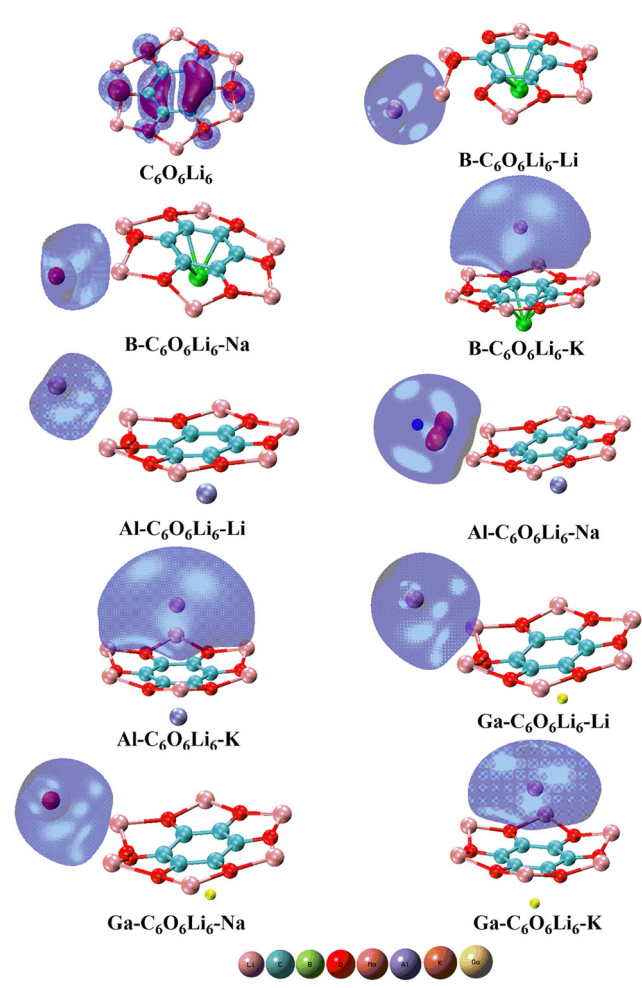
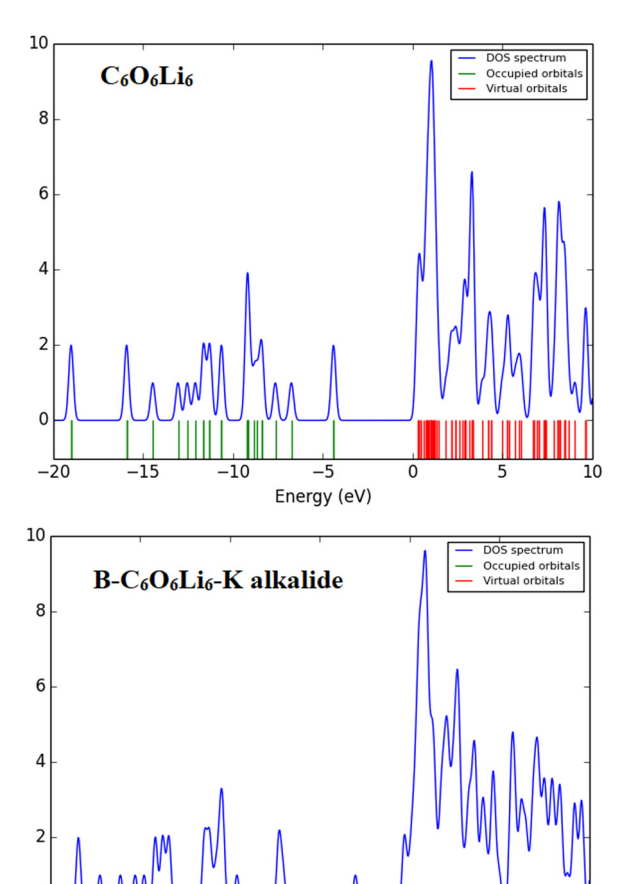


Fig. 3 Pristine C₆O₆Li₆ and group-IA and group-IIIA metal-doped C₆O₆Li₆ alkalides with their highest occupied molecular orbitals.

The stabilization of excess electrons on negatively charged alkali metals is a very crucial factor, which depends on the VIE. These alkalides have VIEs ranging from 3.02 to 3.75 eV to justify their electronic stability. As the VIE increases, it means that the alkalides are stable enough for further synthesis. 79-81 Group-IA metals exhibit a monotonic decreasing trend in VIEs, whereas Group-IIIA metals display a nonmonotonic trend, with the VIE values decreasing from B to Al before increasing again as one moves towards Ga.

The TDOS spectra give information about the occupied and unoccupied orbitals with energy states and electronic interactions in complexes. The total density of states (TDOS) spectra of the designed complexes were studied. These spectra reconfirmed the change in the energy states after complexation compared to individual C6O6Li6. New energy states are generated, and energy gaps are reduced upon complexation, as discussed vide supra in FMO analysis. The intensity of peaks also increases after complexation, which justifies the electronic contribution in each complex, where the overlapping of peaks shows stronger interactions between the Group-IA and Group-IIIA metals and C₆O₆Li₆ (see Fig. 4 and ESI.† Fig. S1).



Energy (eV) Fig. 4 Individual C₆O₆Li₆ and B-C₆O₆Li₆-K alkalides with total density of

-5

-10

NLO analysis of group-IA/IIIA-doped C₆O₆Li₆ alkalides

The geometrical and electronic properties of Group-IA/IIIA metal-doped C₆O₆Li₆ alkalides validate the strong interaction between the selected metals and C₆O₆Li₆. A significant amount of charge transfer occurred. These excess electrons are responsible for the extraordinary NLO response of these alkalides. We also calculated the important NLO parameters to estimate the NLO response of these alkalides such as polarizability (α_0) and hyperpolarizability (β_0). These parameters provide insights into the NLO response. The α_0 and β_0 values were calculated to estimate the NLO response of these alkalides, and the data are given in Table 2. The α_0 value of Groups-IA/IIIA@C₆O₆Li₆ alkalides is in the range of 231 to 800 au, which is remarkably higher than that of pristine C₆O₆Li₆ (137 au). The B-C₆O₆Li₆-K alkalide has the highest α_0 (800 au) and the lowest α_0 (231 au) values found for Ga-C₆O₆Li₆-K. A large amount of charges are transferred (-0.51|e|) from B-C₆O₆Li₆ to the K metal in B-C₆O₆Li₆-K alkalides, which is the crucial factor responsible for the increase in polarizability.¹⁸ In the ongoing work, the α_0 values reflect significant changes in the polarizability of each alkalide because of the interactions between metals and

C₆O₆Li₆. The polarizability increases with the increase in the atomic size of Group-IA metals in each alkalide. Nisar et al. also observed changes in polarizability values during their work on supramolecular assemblies of azobenzene and alkoxystilbazole molecules.82

Besides polarizability, when Groups-IA/IIIA metals are adsorbed on $C_6O_6Li_6$, the β_0 value is considerably increased compared to β_0 (2.89 au) of pristine $C_6O_6Li_6$. The increase in β_0 notifies enhancement in the NLO response of the designed complexes. The β_0 value is in the range of 4.38×10^2 – 1.75×10^5 au for all alkalides by the $\omega B97XD/6-31+G(d,p)$ method. The B-C₆O₆Li₆-K alkalide has the highest β_0 value of 1.75 \times 10⁵ au and B-C₆O₆Li₆-Na has the lowest β_0 value of 4.38×10^2 au. It is observed that the β_0 value increases with the increase in the atomic size of alkali metals. The β_0 results are similar to our previous work on NLO response of alkali metal-doped C6O6Li6 complexes, where the K@C₆O₆Li₆ complex has the highest β_0 value of 2.9×10^5 au compared to other complexes. 42 We see in our present results that K-doped complexes have a higher β_0 value. The second factor is the inverse relationship of energy gap with a β_0 value, and the β_0 value increases with the decrease in energy gap, as observed by Nouman and coworkers during working on alkali metal-doped 2⁶ adamanzane.⁸³ In our study, the B-C₆O₆Li₆-K alkalide has the lowest energy gap of 2.72 eV, but, it has the highest β_0 value of 1.75 \times 10⁵ au. Igbal and coworkers depict from their results on alkaline earth metal-doped adamanzane that the large amount of charge transfer causes an increase in the polarizability of the alkali metal-doped complexes, which causes an increase in hyperpolarizability.84 We also observed that a large amount of charge (-0.51|e|) is transferred to the K metal in B-C₆O₆Li₆-K alkalides, which increases the polarizability and hyperpolarizability of this complex. In the literature, the inverse relationship between the VIE and β_0 values has been reported. VIE of a complex is inversely proportional to hyperpolarizability as observed by Asif et al. upon doping of superalkli with aminated graphdiyne.⁸⁵ VIE is also inversely proportional to β_0 , and B- $C_6O_6Li_6$ -K has the lowest VIE of 3.02 eV and has the highest β_0 . Nisar et al. also observed a change in β_0 values during their work on supramolecular assemblies of azobenzene and alkoxystilbazole molecules.86 We compared the results of our designed B-C₆O₆Li₆-K complex with a number of designed metal-doped complexes reported in the recent literature (see Table 3). This comparative study justifies the better hyperpolarizability result of the B-C₆O₆Li₆-K complex and identifies it to be a good NLO response-generating nanomaterial.

The doped complexes are also analyzed by the LC-BLYP/augcc-PVDZ, \omegaB97XD/aug-cc-PVDZ, LC-BLYP/aug-cc-PVTZ, \omegaB97XD/ aug-cc-PVTZ, LC-BLYP/def2-TZVP, and ωB97XD/def2-TZVP methods. The higher β_0 values are obtained at the ω B97XD/6-31+G(d,p) level, which is given in main manuscript. The NLO parameters including β_0 , α_0 and μ values of other methods are given in the ESI† (ESI.† Table S2). The μ values are between 14.43 and 17.51 Debye, and the α_0 values are up to 507 au and the β_0 values range from 8.89 \times 10² to 1.90 \times 10⁴ au at ω B97XD/aug-cc-PVDZ. The μ values are up to 17.01 Debye, the α_0 values are between 413 and 523 au and the β_0

PCCP Paper

Table 3 Comparative analysis of the hyperpolarizability values of the reported complexes with our best designed B-C₆O₆Li₆-K complex

S. no.	Complexes	Hyperpolarizability (β_0 in au)	Ref.
1.	Superalkali-doped B38	$3.5 imes 10^4$	87
2.	Na@B ₁₂ N ₁₂	$1.89 imes 10^4$	88
3.	Li ₃ O@C ₃₂ H ₁₅ graphene	1.40×10^5	89
4.	$M_1(26 \text{ adz})M_2$ where $(M_1 = M_2 = Be, Mg \text{ and } Ca)$	8.19×10^{3}	84
5.	K@bicorannulenyl (C ₄₀ H ₃₈)	2.68×10^{6}	16
6.	K@B ₁₂ N ₁₁ nanocage	1.3×10^{4}	90
7.	Alkali metal@all-cis-1,2,3,4,5,6-hexafluorocyclohexane F ₆ C ₆ H ₆	$2.91 imes 10^4$	28
8.	Na@2N-atoms functionalized corannulene (C ₁₈ N ₂ H ₁₀)	$4.84 imes 10^4$	91
9.	Ca ₂ @C20 nanocage	$5.86 imes 10^4$	92
10.	K@Boron phosphide	4.41×10^{5}	17
11	$B-C_6O_6Li_6-K$	1.75×10^{5}	Current work

values range from 8.93×10^2 to 2.01×10^4 au at LC-BLYP/aug-cc-PVDZ. The μ values are between 15.99 and 18.31 Debye, the α_0 values are up to 521 au and the β_0 values range from 5.37 \times 10³ to 1.65×10^4 au at ω B97XD/aug-cc-PVTZ. The μ values are up to 18.12 Debye, the α_0 values are between 388 and 503 au and the β_0 values range from 4.04×10^3 to 1.76×10^4 au at LC-BLYP/aug-cc-PVTZ. The μ values are between 5.11 and 17.56 Debye, the α_0 values are up to 762 au and the β_0 values range from 1.16×10^3 to 1.46×10^5 au at ω B97XD/def2-TZVP. The μ values are up to 17.91 Debye, the α_0 values are between 434 and 810 au and the β_0 values range from 2.89×10^3 to 1.29×10^5 au at LC-BLYP/def2-TZVP. The aug-ccPVDZ and aug-cc-PVTZ basis sets show error when implemented on Kcontaining complexes as the atomic size of K is out of reach of these dunning basis sets (aug-ccPVDZ and aug-cc-PVTZ basis sets).

3.5. Two-level model of group-IA/IIIA metal-doped C₆O₆Li₆ alkalides

A two-level model (β_{TLM}) was applied to calculate the internal parameters, which are responsible for the variations in hyperpolarizability (β_0) and ultimately can cause the variation in NLO response (Table 4). These internal parameters are variational dipole moment ($\Delta \mu$), oscillation strength (f_0) and crucial excitation energies. The equation for β_{TLM} is given as follows:

$$\beta_{\rm TLM} = \Delta \mu \times f_0 / \Delta E^3 \tag{11}$$

Table 4 Maximum wavelength (λ_{max} in nm), oscillating strength (f_0), change in excitation energy (ΔE in eV), variation in dipole moment between ground and crucial excited states ($\Delta\mu$ in Debye), hyperpolarizability in au in the two-level model ($\beta_{\rm TLM}$ in au) and hyperpolarizability (β_0 in au) of pristine C₆O₆Li₆ and Group-I and Group-III metal-doped C₆O₆Li₆alkalides (group-I = K, Na, and Li; group-III = Ga, Al, and B)

Parameters	λ_{max}	f_0	ΔE	$\Delta \mu$	β_{TLM}	β_0
C ₆ O ₆ Li ₆	515	0.03	2.42	0.01	0.000	2.89
B-C ₆ O ₆ Li ₆ -Li	580	0.43	2.14	-0.14	-0.006	1.11×10^4
B-C ₆ O ₆ Li ₆ -Na	606	0.38	2.05	-0.08	-0.004	4.38×10^{2}
B-C ₆ O ₆ Li ₆ -K	1556	0.41	0.80	0.04	0.032	1.75×10^{5}
Al-C ₆ O ₆ Li ₆ -Li	629	0.41	1.97	-0.1	-0.005	9.06×10^{3}
Al-C ₆ O ₆ Li ₆ -Na	654	0.38	1.90	-0.09	-0.005	9.39×10^{3}
Al-C ₆ O ₆ Li ₆ -K	1393	0.42	0.89	0.04	0.024	7.50×10^{4}
Ga-C ₆ O ₆ Li ₆ -Li	602	0.40	0.83	1.71	0.076	$1.26 imes 10^5$
Ga-C ₆ O ₆ Li ₆ -Na	625	0.39	1.98	1.69	0.085	7.49×10^{3}
Ga-C ₆ O ₆ Li ₆ -K	1375	0.44	0.90	1.06	0.640	7.17×10^4

These changes in dipole moment between the ground state and the crucial excited state dipole moment $(\Delta \mu)$ and oscillation strength (f_0) are directly correlated with β_{TLM} and crucial excitation energies to this β_{TLM} . ⁹³ The $\Delta\mu$ values lie between -0.08 and 1.71 Debye, whereas f_0 ranges from 0.38 to 0.44. The trend of increase in f_0 is opposite to β_0 . The trend of change in dipole moment is similar to β_0 in each complex. In B-C₆O₆Li₆, K-doped B-C₆O₆Li₆ has a higher $\Delta\mu$ value (0.04 Debye) and it also has large β_0 (1.75 \times 10⁵ au). Similarly in Al-C₆O₆Li₆, Kdoped Al-C₆O₆Li₆ has a higher $\Delta\mu$ value (0.04 Debye) and it also has large β_0 (7.50 × 10⁴ au). Then in Ga-C₆O₆Li₆, Li-doped $Ga-C_6O_6Li_6$ has a higher $\Delta\mu$ value (1.76 Debye) and it also has large β_0 (1.26 × 10⁵ au).

The trend of decrease in excitation energy values is comparable to β_0 in each complex. In B-C₆O₆Li₆, K-doped B-C₆O₆Li₆ has the lowest ΔE value (0.80 eV) and has the largest β_0 $(1.75 \times 10^5 \text{ au})$. Similarly in Al-C₆O₆Li₆, K-doped Al-C₆O₆Li₆ has a lower ΔE value (0.89 eV) and it also has large β_0 (7.50 \times 10⁴ au). Exceptional behavior is seen in Ga-C₆O₆Li₆ where Lidoped Ga-C₆O₆Li₆ has a lower ΔE value (0.83 eV) and a larger β_0 value (1.26 \times 10⁵ au). The excitation energy plays a key role in increasing the hyperpolarizability of alkalides. The β_0 value of B-C₆O₆Li₆-K is 1.75×10^5 au, which has the lowest excitation energy of 0.80 eV among the investigated alkalides, which is in accordance with the two-level model. These results indicated that the excitation energy is responsible for the enhancement of NLO response. Overall, the increasing trend of β_{TLM} is comparable to β_0 , and β_{TLM} outcomes support our results. Similar results have also been previously reported for superalkalidoped graphdiyne by Kosar et al. in the literature. 94

3.6. Vibrational frequency-dependent first hyperpolarizability of group-I/IIIA metal-doped C₆O₆Li₆ alkalides

We also analyzed the frequency-dependent first hyperpolarizability to illustrate the vibrational frequency-dependent behavior of wave function on NLO response, as previously reported by Kirtman et al. in the literature. 95 Two important coefficients including second-harmonic generation (SHG represented $\beta(-2\omega;\omega,\omega)$) and electro optic Pockel effect (EOPE represented $-\beta(-\omega; \omega, 0)$ coefficients were obtained. These coefficients were calculated at two frequencies mostly used in laser technology, 96,97 and their values are given in Table 5.

Table 5 Coefficients of vibrational frequency-dependent first hyperpolarizability ($\beta(\omega)$), i.e., electro-optic Pockel's effect $\beta_0(-\omega; \omega, 0)$ and second $harmonic \ generation \ \beta_0(-2\omega;\omega,\omega) \ with \ static \ first \ hyperpolarizability \ \beta_0(0;0,0) \ in \ au \ calculated \ at \ \omega B97XD/6-31+G(d,p) \ of \ pristine \ C_6O_6Li_6 \ and \ group-I_6-200 \ and \ group-I_6-200$ and group-III metal-doped $C_6O_6Li_6$ -alkalides (group-I = K, Na, and Li; group-III = Ga, Al, and B)

Pristine and doped complexes	Frequency	$\beta_0(0; 0, 0)$	$\beta_0(-\omega; \omega, 0)$	$\beta_0(-2\omega;\omega,\omega)$
$C_6O_6Li_6$	0	2.89×10^{0}		
	532		$9.20 imes 10^2$	3.63×10^{1}
	1064		3.06×10^0	2.02×10^{1}
B-C ₆ O ₆ Li ₆ -Li	0	1.11×10^4		
	532		2.41×10^{7}	$8.62 imes 10^5$
	1064		4.37×10^{3}	4.76×10^{5}
B-C ₆ O ₆ Li ₆ -Na	0	4.38×10^2		
	532		2.02×10^{6}	$9.12 imes 10^4$
	1064		1.36×10^4	7.02×10^5
$B-C_6O_6Li_6-K$	0	1.75×10^5		
	532		1.78×10^{8}	1.71×10^{7}
	1064		4.98×10^6	8.84×10^{6}
$Al-C_6O_6Li_6-Li$	0	9.06×10^{3}		
0 0 0	532		2.28×10^{7}	7.45×10^{4}
	1064		2.29×10^4	1.36×10^5
Al-C ₆ O ₆ Li ₆ -Na	0	9.39×10^3		
	532		1.82×10^{6}	1.69×10^{6}
	1064		3.87×10^4	5.42×10^5
Al-C ₆ O ₆ Li ₆ -K	0	$7.50 imes 10^4$		
	532		5.33×10^{5}	$4.11 imes 10^4$
	1064		5.67×10^5	3.15×10^5
$Ga-C_6O_6Li_6-Li$	0	1.26×10^5		
	532		6.48×10^{5}	7.07×10^{4}
	1064		1.39×10^4	4.21×10^5
Ga-C ₆ O ₆ Li ₆ -Na	0	7.49×10^3		
	532		5.97×10^{6}	9.24×10^{7}
	1064		1.02×10^4	3.05×10^{5}
Ga-C ₆ O ₆ Li ₆ -K	0	7.17×10^{4}		
	532		6.94×10^{5}	7.31×10^{4}
	1064		5.51×10^5	5.17×10^{5}

This Table illustrates that the change in frequency caused a prominent increase in first hyperpolarizability, which described a significant enhancement in NLO response at both frequencies (532 and 1064 nm). Static hyperpolarizability ranges from 4.38×10^2 to 1.75×10^5 au. The SHG values for all designed nine complexes are between 4.11×10^4 and 9.24×10^4 10⁷ au and the EOPE values for all the designed nine complexes are between 5.33×10^5 and 1.78×10^8 au at 532 nm. The SHG values for all the designed nine complexes are between 1.36 \times 10^5 and 8.84×10^6 au and the EOPE values for all the designed nine complexes are between 4.37×10^3 and 4.98×10^6 au at 1064 nm. The higher EOPE (9.24 \times 10⁷ au) and SHG (1.78 \times 10⁸ au) values were obtained for B-C₆O₆Li₆-K and B-C₆O₆Li₆-K complexes. These results described the prominent EOPE and SHG effects at a lower frequency of 532 nm.

3.7. Static and vibrational frequency-dependent second hyperpolarizability of group-I/IIIA metal-doped C₆O₆Li₆ alkalides

We further elaborate our study by analyzing the static $(\gamma(0))$ and frequency-dependent second hyperpolarizability ($\gamma(\omega)$). Two important coefficients including electric field-induced secondharmonic generation $(\gamma(-2\omega; \omega, \omega, 0))$ represented by ESHG, and the dc Kerr effect $(\gamma(-\omega; \omega, \omega, 0))$ coefficients were calculated at 532 and 1064 nm frequencies. The values of these coefficients are given in Table 6.

This table illustrates that the change in frequency caused a valuable increase in second hyperpolarizability, which described a significant enhancement in NLO response at both frequencies (532 and 1064 nm). The static, dc Karr and EFSHG values for pristine $C_6O_6Li_6$ are 5.21×10^6 , 3.69×10^8 and 3.12×10^8 10⁷ au, respectively. After complexations, the static hyperpolarizability values range from 4.11×10^6 to 5.31×10^7 au. The EFSHG values for all designed nine complexes are between 9.57×10^7 and 2.09×10^{10} au and the dc Karr effect values for all designed nine complexes are between 1.33×10^8 and $2.90 \times$ 1011 au at 532 nm. The SHG values for all the designed nine complexes are between 8.80×10^6 and 1.13×10^{10} au and the EOPE values for all the designed nine complexes are between 3.08×10^5 and 1.26×10^9 au at 1064 nm. The higher dc Karr effect (2.90 \times 10¹¹ au) and EFSHG (2.09 \times 10¹⁰ au) values were obtained for B-C₆O₆Li₆-Na and Al-C₆O₆Li₆-Na complexes.

Table 6 Coefficients of vibrational frequency-dependent second hyperpolarizability $(\gamma(\omega))$, i.e., electric field-induced second-harmonic generation (SHG) with $\beta(-2\omega; \omega, \omega, \omega)$ term, the electro-optical Karr effect (EOKE) with $(\beta(-\omega; \omega, 0, 0))$ term with static second hyperpolarizability $(\gamma(0))$ in au, and nonlinear refractive index $(n_2$ in cm W⁻¹) calculated at ωB97XD/6-31+G(d,p) of pristine C₆O₆Li₆ and group-I and group-III metal-doped C₆O₆Li₆-alkalides (group-I = K, Na, and Li; group-III = Ga, Al, and B)

Pristine and doped complexes	Frequency	$\gamma_0(0; 0, 0, 0)$	$\gamma_0(-\omega; \omega, \omega, 0)$	$\gamma_0(-2\omega;\omega,\omega)$	n_2
$C_6O_6Li_6$	0	5.21×10^{6}			
	532		3.69×10^{8}	9.52×10^{8}	3.66×10^{-14}
	1064		3.12×10^7	4.04×10^7	2.12×10^{-15}
B-C ₆ O ₆ Li ₆ -Li	0	4.11×10^6			
	532		1.95×10^8	9.33×10^{8}	3.12×10^{-14}
	1064		2.28×10^{7}	4.44×10^{7}	1.97×10^{-15}
B-C ₆ O ₆ Li ₆ -Na	0	5.31×10^{7}			
0 0 0	532		2.90×10^{11}	1.39×10^{10}	8.39×10^{-12}
	1064		1.26×10^9	1.13×10^{10}	3.48×10^{-13}
B-C ₆ O ₆ Li ₆ -K	0	$4.43 imes 10^6$			
6 - 66	532		7.18×10^{8}	9.57×10^{7}	2.26×10^{-14}
	1064		2.35×10^{7}	1.02×10^8	3.59×10^{-15}
Al-C ₆ O ₆ Li ₆ -Li	0	$6.25 imes 10^6$			
-0-0-0	532	***************************************	1.15×10^{9}	1.99×10^{10}	5.81×10^{-13}
	1064		4.69×10^{7}	2.77×10^{8}	9.11×10^{-15}
Al-C ₆ O ₆ Li ₆ -Na	0	3.00×10^{7}			
-6-6-6-1	532		1.47×10^{9}	2.09×10^{9}	9.91×10^{-14}
	1064		1.48×10^{8}	3.14×10^8	1.36×10^{-14}
$\mathrm{Al-C_6O_6Li_6-}\mathrm{K}$	0	$4.55 imes 10^6$			
	532	-1000	$8.00 imes 10^8$	1.23×10^{9}	5.62×10^{-14}
	1064		2.37×10^{7}	9.76×10^{7}	3.47×10^{-15}
Ga-C ₆ O ₆ Li ₆ -Li	0	6.41×10^{6}			
	532	0.11 / 10	6.46×10^{8}	9.27×10^{8}	4.36×10^{-14}
	1064		4.81×10^7	3.40×10^{8}	1.09×10^{-14}
Ga-C ₆ O ₆ Li ₆ -Na	0	2.97×10^{7}			
Su Sporting The	532		$4.05 imes 10^8$	1.94×10^8	1.74×10^{-14}
	1064		1.56×10^8	3.24×10^8	1.41×10^{-14}
Ga-C ₆ O ₆ Li ₆ -K	0	1.45×10^{5}			
	532	1.10 // 10	1.33×10^{8}	2.67×10^{8}	1.10×10^{-14}
	1064		3.08×10^{5}	8.80×10^{6}	2.55×10^{-16}

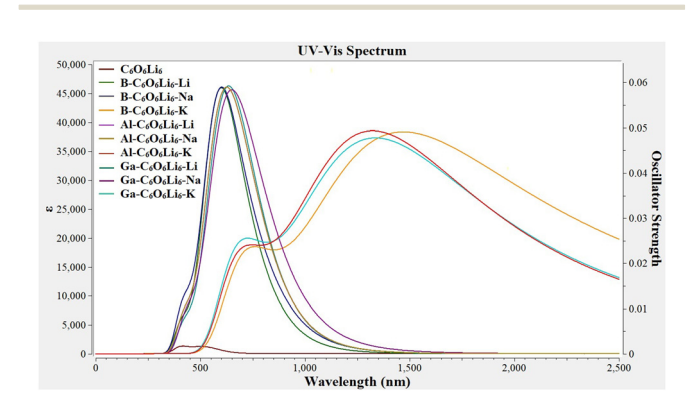
These results depict the prominent EOPE and EFSHG effects at a lower frequency of 532 nm. Similar results were obtained by Mahmood and coworkers, which also show the higher vibrational frequency-dependent first and second hyperpolarizability values at 532 nm. 98

The nonlinear refractive index (n_2) of Group IA/IIIA-doped $C_6O_6Li_6$ range from 8.39×10^{-12} to 2.55×10^{-16} cm 2 W $^{-1}$. The higher n_2 value $(8.39 \times 10^{-12}$ cm 2 W $^{-1}$) was obtained for B-C₆O₆Li₆-Na at 532 nm and the lower n_2 value $(2.55 \times 10^{-16}$ cm 2 W $^{-1})$ was obtained for Ga-C₆O₆Li₆-K at 1064 nm. The charge transfer from Group-IIIA to Group-IA metals occurs through $C_6O_6Li_6$ in a complex. The excess charge transfer within this complex causes polarization, which can possibly be responsible for the increase in nonlinear refractive index and enhancement of NLO response, as previously reported in the literature.

3.8. TD-DFT calculation of group-I/IIIA metal-doped ${\rm C_6O_6Li_6}$ alkalides

The absorption maxima (λ_{max}) of Group-IIIA-C₆O₆Li₆-Group-IA range from 580 to 1556 nm, where the highest value (1556 nm)

is observed for B–C₆O₆Li₆–K and the lowest value (580 nm) is observed for B–C₆O₆Li₆–Li alkalides (see Fig. 5). All these values are higher than those of pristine C₆O₆Li₆ (λ_{max} = 515 nm). K-Doped Group-IIIA-C₆O₆Li₆ has a higher wavelength than that of



 $\begin{array}{lll} \textbf{Fig. 5} & \textbf{Ultra-violet-visible (UV-vis) spectra of pristine $C_6O_6Li_6$ and group-I and group-III metal-doped $C_6O_6Li_6$-alkalides (group-I = K, Na, and Li; group-III = Ga, Al, and B). \end{array}$

Na and Li doped alkalides. The outcomes of UV-vis analysis are comparable to the research report on NLO response of alkali metal-doped C₆O₆Li₆ complexes, where K-C₆O₆Li₆-Mg complex has the highest λ_{max} value among all selected alkali metaldoped C₆O₆Li₆ complexes. ⁴¹ These results show bathochromic shifts in all alkalides. Comparable red shift behavior of Group I/ IIIA metal-doped complexes 92,95 reported in the literature justifies our results.

4. Conclusion

Metals act as sources of excess electrons that enhance the nonlinear optical (NLO) response of complexes. The NLO response of C₆O₆Li₆ was evaluated with Group IA (K, Na, and Li) and Group IIIA (Ga, Al, and B) metals. In these alkalides, π conjugation of C₆O₆Li₆ withdraws excess electrons from Group IIIA metals, which are transferred to Group IA metals. All alkalides are thermodynamically stable, with the internal energy (E_{int}) increasing to -109.13 kcal mol⁻¹ after complexation. The vertical ionization energies (VIEs) of 3.75 eV and 3.02 eV indicate electronic stability. Charge analysis shows positive charges on Group IIIA and negative charges on Group IA metals, with HOMO densities on anionic Group IA metals confirming alkalide properties. The semiconducting behavior is evident from HOMO-LUMO energy gaps compared to pristine C₆O₆Li₆. The NLO response, characterized by hyperpolarizability, is highest in the B-C₆O₆Li₆-K alkalide, with the highest β_0 of 1.75 \times 10⁵ au. A two-level model elucidates changes in the first hyperpolarizability due to excitation energy and dipole moment variations. The vibrational frequencydependent first and second hyperpolarizability values were also calculated, which depicts the increase in hyperpolarizability values at a frequency of 532 nm. The higher n_2 value (8.39 \times 10^{-12} cm² W⁻¹) was obtained for B-C₆O₆Li₆-Na at 532 nm. The UV-vis analysis confirms a bathochromic shift in all alkalides, marking them as promising candidates for future electronics with significant NLO responses.

Data availability

The data supporting the findings of this study are available from the corresponding author mahmood@cuiatd.edu.pk (T. M) upon reasonable request.

Conflicts of interest

There are no conflicts to declare.

Acknowledgements

The authors acknowledge the Higher Education Commission (NRPU project; 20-16279/NRPU/HEC/2021-2020) of Pakistan. M. I express appreciation to the Deanship of Scientific Research at King Khalid University Saudi Arabia through the research groups program under Grant Number RGP1/86/44. The experiments presented in this paper were carried out using the facilities of the Benefit Advanced AI and Computing Lab at the University of Bahrain—see https://ailab.uob.edu.bh with support from Benefit Bahrain Company—see https://ben efit.bh.

References

- 1 H. Ai, Y. Bu, P. Li and L. Sun, J. Phys. Chem. A, 2004, 108, 4156-4162.
- 2 R.-L. Zhong, H.-L. Xu, Z.-R. Li and Z.-M. Su, J. Phys. Chem. Lett., 2015, 6, 612-619.
- 3 Y. Bai, Z.-J. Zhou, J.-J. Wang, Y. Li, D. Wu, W. Chen, Z.-R. Li and C.-C. Sun, J. Phys. Chem. A, 2013, 117, 2835-2843.
- 4 W.-M. Sun, X.-H. Li, J. Wu, J.-M. Lan, C.-Y. Li, D. Wu, Y. Li and Z.-R. Li, Inorg. Chem., 2017, 56, 4594-4600.
- 5 A. Ahsin and K. Ayub, Mater. Sci. Semicond. Process., 2022, 138, 106254.
- 6 R. Zheng, B. Zhang, C. Wang and J. Hou, New J. Chem., 2022, 46, 15334-15343.
- 7 Y. Y. Liang, B. Li, X. Xu, F. Long Gu and C. Zhu, J. Comput. Chem., 2019, 40, 971-979.
- 8 N. Maqsood, A. Asif, K. Ayub, J. Iqbal, A. Y. Elnaggar, G. A. M. Mersal, M. M. Ibrahim and S. M. El-Bahy, RSC Adv., 2022, 12, 16029-16045.
- 9 P. Khan, T. Mahmood, K. Ayub, S. Tabassum and M. Amjad Gilani, Opt. Laser Technol., 2021, 142, 107231.
- 10 L. Dalton, M. Lauermann and C. Koos, NLO: Electro-Optic Applications, 2016, 369-396.
- 11 S. Di Bella, I. Fragalà, I. Ledoux, M. A. Diaz-Garcia and T. J. Marks, J. Am. Chem. Soc., 1997, 119, 9550-9557.
- 12 V. Parodi, E. Jacchetti, R. Osellame, G. Cerullo, D. Polli and M. T. Raimondi, Front. Bioeng. Biotechnol., 2020, 8, 585363.
- 13 T. Tian, Y. Fang, W. Wang, M. Yang, Y. Tan, C. Xu, S. Zhang, Y. Chen, M. Xu, B. Cai and W.-Q. Wu, Nat. Commun., 2023, 14, 4429.
- 14 N. Li, J. Lu, H. Li and E.-T. Kang, Dyes Pigm., 2011, 88, 18-24.
- 15 R. Kaur, K. P. Singh and S. K. Tripathi, J. Alloys Compd., 2022, 905, 164103.
- 16 A. Parveen, J. Yagoob, S. Ijaz, R. Baloach, M. U. Khan, R. Hussain, H. M. Abo-Dief, A. K. Alanazi and Z. M. El-Bahy, ChemistrySelect, 2023, 8(21), e202300843.
- 17 M. Rashid, J. Yaqoob, N. Khalil, R. Jamil, M. U. Khan and M. A. Gilani, Mater. Sci. Semicond. Process., 2022, 151, 107007.
- 18 N. Kosar, H. Tahir, K. Ayub, M. A. Gilani, M. Imran and T. Mahmood, Mater. Sci. Semicond. Process., 2022, 138, 106269.
- 19 W. Jin, C. Xie, X. Hou, M. Cheng, E. Tikhonov, M. Wu, S. Pan and Z. Yang, Chem. Mater., 2023, 35, 5281-5290.
- 20 N. Hou and X.-H. Fang, Inorg. Chem., 2022, 61, 10756-10767.
- 21 X. Li, J. Mater. Chem. C, 2018, 6, 7576-7583.

- 22 F. Ullah, N. Kosar, A. Ali, Maria, T. Mahmood and K. Ayub, Phys. E, 2020, 118, 113906.
- 23 S. Taboukhat, N. Kichou, J.-L. Fillaut, O. Alévêque, K. Waszkowska, A. Zawadzka, A. El-Ghayoury, A. Migalska-Zalas and B. Sahraoui, *Sci. Rep.*, 2020, 10, 15292.
- 24 N. Kosar, T. Mahmood, K. Ayub, S. Tabassum, M. Arshad and M. A. Gilani, Opt. Laser Technol., 2019, 120, 105753.
- 25 N. Kosar, K. Shehzadi, K. Ayub and T. Mahmood, *Optik*, 2020, **218**, 165033.
- 26 Y.-F. Wang, J. Huang, L. Jia and G. Zhou, J. Mol. Graphics Model., 2014, 47, 77–82.
- 27 X. Lu, L. Feng, T. Akasaka and S. Nagase, *Chem. Soc. Rev.*, 2012, 41, 7723.
- 28 A. Ahsin, A. Ali and K. Ayub, J. Mol. Graphics Model., 2020, 101, 107759.
- 29 M. A. Alkhalifah, N. S. Sheikh, Y. S. S. Al-Faiyz, I. Bayach, R. Ludwig and K. Ayub, *Materials*, 2023, **16**, 3447.
- 30 A. Ahsin, A. Ali and K. Ayub, *Mater. Sci. Semicond. Process.*, 2023, **162**, 107506.
- 31 G. Serdaroğlu, N. Uludag, P. Sugumar and P. Rajkumar, *J. Mol. Struct.*, 2021, **1244**, 130978.
- 32 W.-M. Sun, D. Wu, Y. Li, J.-Y. Liu, H.-M. He and Z.-R. Li, *Phys. Chem. Chem. Phys.*, 2015, 17, 4524–4532.
- 33 X. Li and S. Li, J. Mater. Chem. C, 2019, 7, 1630-1640.
- 34 W. Chen, Z. R. Li, D. Wu, Y. Li, C. C. Sun, F. L. Gu and Y. Aoki, *J. Am. Chem. Soc.*, 2006, **128**, 1072–1073.
- 35 W.-M. Sun, L.-T. Fan, Y. Li, J.-Y. Liu, D. Wu and Z.-R. Li, *Inorg. Chem.*, 2014, 53, 6170-6178.
- 36 W.-M. Liang, Z.-X. Zhao, D. Wu, W.-M. Sun, Y. Li and Z.-R. Li, *J. Mol. Model.*, 2015, **21**, 311.
- 37 P. Banerjee and P. K. Nandi, Struct. Chem., 2018, 29, 859–870.
- 38 D. Kang, L. Zhao, Z.-M. Su and H.-L. Xu, J. Mol. Liq., 2023, 385, 122400.
- 39 Y.-F. Wang, J. Li, J. Huang, T. Qin, Y.-M. Liu, F. Zhong, W. Zhang and Z.-R. Li, J. Phys. Chem. C, 2019, 123, 23610–23619.
- 40 M. Sohaib, H. Sajid, S. Sarfaraz, M. H. S. A. Hamid, M. A. Gilani, M. Ans, T. Mahmood, S. Muhammad, M. A. Alkhalifah, N. S. Sheikh and K. Ayub, *Heliyon*, 2023, 9, e19325.
- 41 N. Kosar, S. Wajid, K. Ayub, M. A. Gilani, N. H. Binti Zainal Arfan, M. H. Sheikh Abdul Hamid, M. Imran, N. S. Sheikh and T. Mahmood, *Heliyon*, 2023, **9**, e18264.
- 42 S. Wajid, N. Kosar, F. Ullah, M. A. Gilani, K. Ayub, S. Muhammad and T. Mahmood, *ACS Omega*, 2021, 6, 29852–29861.
- 43 N. Kosar, S. Wajid, K. Ayub, M. A. Gilani and T. Mahmood, *Chem. Phys.*, 2023, **570**, 111894.
- 44 N. Kosar, S. Wajid, K. Ayub and T. Mahmood, *Optik*, 2023, **276**, 170660.
- 45 N. Kosar, L. Zari, K. Ayub, M. A. Gilani and T. Mahmood, *Phys. Scr.*, 2023, **98**, 065909.
- 46 D. Gounden, N. Nombona and W. E. van Zyl, *Coord. Chem. Rev.*, 2020, **420**, 213359.

- 47 R. Sreedharan, S. Ravi, K. R. Raghi, T. K. M. Kumar and K. Naseema, *SN Appl. Sci.*, 2020, 2, 578.
- 48 M. Aetizaz, F. Ullah, T. Mahmood and K. Ayub, *Comput. Theor. Chem.*, 2024, **1232**, 114469.
- 49 S. Kaviani, I. Piyanzina, O. V. Nedopekin and D. A. Tayurskii, *Int. J. Hydrogen Energy*, 2023, **48**, 30069–30084.
- 50 M. A. Adebisi, C.-D. Chen, M. Maaza, C. Ronning, E. Manikandan, D. E. Motaung, P. S. Christopher, K. Bharuth-Ram, N. S. Aliyu, M. N. Pillay and M. K. Moodley, *Phys. Status Solidi*, 2023, 220(1), 2200464.
- 51 Y. Deng and J. Jiang, IEEE Sens. J., 2022, 22, 13811-13834.
- 52 X. Zhang and J. Meng, *Ultra-Wide Bandgap Semiconductor Materials*, Elsevier, 2019, pp. 347–419.
- 53 H. Hora, J. Energy Power Eng., 2020, 14, 156-177.
- 54 M. J. Frisch, G. W. Trucks, H. B. Schlegel, G. E. Scuseria, M. A. Robb, J. R. Cheeseman, G. Scalmani, V. Barone, B. Mennucci, G. A. Petersson, H. Nakatsuji, M. Caricato, X. Li, H. P. Hratchian, A. F. Izmaylov, J. Bloino, G. Zheng, J. L. Sonnenberg, M. Hada, M. Ehara, K. Toyota, R. Fukuda, J. Hasegawa, M. Ishida, T. Nakajima, Y. Honda, O. Kitao, H. Nakai, T. Vreven, J. A. Montgomery Jr., J. E. Peralta, F. Ogliaro, M. Bearpark, J. J. Heyd, E. Brothers, K. N. Kudin, V. N. Staroverov, R. K. J. Normand, K. Raghavachari, A. Rendell, J. C. Burant, S. S. Iyengar, J. Tomasi, M. C. N. Rega, J. M. Millam, M. Klene, J. E. Knox, J. B. Cross, V. Bakken, C. Adamo, J. J. R. Gomperts, R. E. Stratmann, O. Yazyev, A. J. Austin, R. Cammi, C. Pomelli, J. W. Ochterski, R. L. Martin, K. Morokuma, V. G. Zakrzewski, G. A. Voth, P. Salvador, J. J. Dannenberg, S. Dapprich, A. D. Daniels, O. Farkas, J. B. Foresman, J. V. Ortiz and J. D. J. F. Cioslowski, Gaussian 09, Revision D.01, Gaussian, Inc., Wallingford CT, 2009.
- 55 R. I. Dennington, T. Keith and J. Millam, *GaussView version* 5.0.8, semichem, Inc., Shawnee Mission, KS, 2008.
- 56 S. Tariq, A. R. Raza, M. Khalid, S. L. Rubab, M. U. Khan, A. Ali, M. N. Tahir and A. A. C. Braga, *J. Mol. Struct.*, 2020, 1203, 127438.
- 57 N. Islam and A. H. Pandith, J. Mol. Model., 2014, 20, 2535.
- 58 D. R. Mohbiya and N. Sekar, *ChemistrySelect*, 2018, **3**, 1635–1644.
- 59 M. Sherafati, A. Shokuhi Rad, M. Ardjmand, A. Heydarinasab, M. Peyravi and M. Mirzaei, Curr. Appl. Phys., 2018, 18, 1059–1065.
- 60 N. Hou, Y.-Y. Wu and J.-Y. Liu, *Int. J. Quantum Chem.*, 2016, **116**, 1296–1302.
- 61 Z. Liu, J. Sun, C. Yan, Z. Xie, G. Zhang, X. Shao, D. Zhang and S. Zhou, *J. Mater. Chem. C*, 2020, **8**, 12993–13000.
- 62 P. S. Halasyamani and J. M. Rondinelli, *Nat. Commun.*, 2018, **9**, 2972.
- 63 M. Tarazkar, D. A. Romanov and R. J. Levis, J. Phys. B: At., Mol. Opt. Phys., 2015, 48, 094019.
- 64 C. Bree, A. Demircan and G. Steinmeyer, *IEEE J. Quantum Electron.*, 2010, **46**, 433–437.
- 65 H. Iikura, T. Tsuneda, T. Yanai and K. Hirao, *J. Chem. Phys.*, 2001, **115**, 3540–3544.
- 66 T. H. Dunning, J. Chem. Phys., 1989, 90, 1007-1023.
- 67 R. A. Kendall, T. H. Dunning and R. J. Harrison, *J. Chem. Phys.*, 1992, **96**, 6796–6806.

- 68 F. Weigend, Phys. Chem. Chem. Phys., 2006, 8, 1057.
- 69 F. Weigend and R. Ahlrichs, Phys. Chem. Chem. Phys., 2005, 7, 3297.
- 70 Maria, J. Iqbal, R. Ludwig and K. Ayub, Mater. Res. Bull., 2017, 92, 113-122.
- 71 D. R. Kanis, M. A. Ratner and T. J. Marks, Chem. Rev., 1994, 94, 195-242.
- 72 X. Zhang, G. Liu, K. Meiwes-Broer, G. Ganteför and K. Bowen, Angew. Chemie, 2016, 128, 9796-9799.
- 73 A. Ahsan and K. Ayub, J. Mol. Liq., 2020, 297, 111899.
- 74 K. Srinivasu and S. K. Ghosh, J. Phys. Chem. C, 2012, 116, 5951-5956.
- 75 Y. Arshad, S. Khan, M. A. Hashmi and K. Ayub, New J. Chem., 2018, 42, 6976-6989.
- 76 J. Kotakoski, C. H. Jin, O. Lehtinen, K. Suenaga and A. V. Krasheninnikov, Phys. Rev. B: Condens. Matter Mater. Phys., 2010, 82, 113404.
- 77 W.-M. Liang, Z.-X. Zhao, D. Wu, W.-M. Sun, Y. Li and Z.-R. Li, J. Mol. Model., 2015, 21, 311.
- 78 P. Khan, T. Mahmood, K. Ayub, S. Tabassum and M. Amjad Gilani, Opt. Laser Technol., 2021, 142, 107231.
- 79 V. Galasso, B. Kovač, A. Modelli, M. F. Ottaviani and F. Pichierri, J. Phys. Chem. A, 2008, 112, 2331-2338.
- 80 M.-S. Liao, J. D. Watts and M.-J. Huang, J. Phys. Chem. C, 2014, 118, 21911-21927.
- 81 D. W. Boukhvalov, A. N. Rudenko, D. A. Prishchenko, V. G. Mazurenko and M. I. Katsnelson, Phys. Chem. Chem. Phys., 2015, 17, 15209-15217.
- 82 A. Nisar, S. Tabassum, K. Ayub, T. Mahmood, H. AlMohamadi, A. L. Khan, M. Yasin, R. Nawaz and M. A. Gilani, Phys. Chem. Chem. Phys., 2023, 25, 20430-20450.
- 83 R. Akbar, A. Asif, N. Magsood and M. Nouman, Struct. Chem., 2024, 35, 1943-1962.
- 84 A. Rafique, H. Maqbool, R. A. Shehzad, I. A. Bhatti, K. Ayub, A. Elmushyakhi, A. M. Shawky and J. Igbal, Int. J. Quantum Chem., 2023, 123(6), e27060.
- 85 M. Asif, H. Sajid, K. Ayub, M. A. Gilani and T. Mahmood, Polyhedron, 2022, 215, 115695.

- 86 A. Nisar, S. Tabassum, K. Ayub, T. Mahmood, H. AlMohamadi, A. L. Khan, M. Yasin, R. Nawaz and M. A. Gilani, Phys. Chem. Chem. Phys., 2023, 25, 20430-20450.
- 87 M. U. Khan, M. R. S. A. Janjua, J. Yaqoob, R. Hussain, M. Khalid, A. Syed, A. M. Elgorban and N. S. S. Zaghloul, J. Photochem. Photobiol., A, 2023, 440, 114667.
- 88 N. Hou, Y.-Y. Wu and J.-Y. Liu, Int. J. Quantum Chem., 2016, 116, 1296-1302.
- 89 N. Kosar, K. Ayub and T. Mahmood, J. Mol. Graphics Model., 2021, 102, 107794.
- 90 Maria, J. Igbal and K. Ayub, J. Alloys Compd., 2016, 687, 976-983.
- 91 R. Nazir, J. Yaqoob, M. U. Khan, M. A. Gilani, R. Hussain, M. U. Alvi, M. Rashid, M. A. Assiri and M. Imran, Phys. B, 2022, 640, 414041.
- 92 N. Kosar, H. Tahir, K. Ayub, M. A. Gilani, M. Arshad and T. Mahmood, Comput. Theor. Chem., 2021, 1204, 113386.
- 93 Z.-G. Shao and Z.-L. Sun, *Phys. E*, 2015, 74, 438–442.
- 94 N. Kosar, K. Shehzadi, K. Ayub and T. Mahmood, J. Mol. Graphics Model., 2020, 97, 107573.
- 95 N. Kosar, S. Gul, K. Ayub, A. Bahader, M. A. Gilani, M. Arshad and T. Mahmood, Mater. Chem. Phys., 2020, 242, 122507.
- 96 S. Muhammad, A. G. Al-Sehemi, Z. Su, H. Xu, A. Irfan and A. R. Chaudhry, J. Mol. Graphics Model., 2017, 72, 58-69.
- 97 A. Plaquet, B. Champagne and F. Castet, Molecules, 2014, 19, 10574-10586.
- 98 N. Kosar, S. Kanwal, H. Sajid, K. Ayub, M. A. Gilani, K. Elfaki Ibrahim, M. K. Gatasheh, Y. S. Mary and T. Mahmood, J. Mol. Graphics Model., 2024, 126, 108646.
- 99 N. Kosar, S. Kanwal, H. Sajid, K. Ayub, M. A. Gilani, K. Elfaki Ibrahim, M. K. Gatasheh, Y. S. Mary and T. Mahmood, J. Mol. Graphics Model., 2024, 126, 108646.
- 100 J. Yaqoob, T. Mahmood, K. Ayub, S. Tabassum, A. F. Khan, S. Perveen, J. Yang and M. A. Gilani, Eur. Phys. J. Plus, 2022, 137, 233.
- 101 X. Zhou, C. Zhao, G. Wu, J. Chen and Y. Li, Appl. Surf. Sci., 2018, 459, 354-362.